


FULL PAPER

Open Access



Influence of low-velocity superficial layer on long-period basin-induced surface waves in eastern Osaka basin

Ivo Oprsal^{1,2*} , Haruko Sekiguchi³, Tomotaka Iwata³ and Jan Burjanek¹

Abstract

The long-period strong ground motions with periods above 1 s have, in the case of farther or deeper earthquakes, potential to cause serious damage to structures with low eigen frequency, such as long bridges, oil tanks, or artificially damped structures, such as high-rise buildings. This work focuses on wave propagation due to the deep large earthquake representing rare deep damaging events of the region, with relatively sparse data coverage, studied for simple geological models computed by 2D finite differences. We model the wave propagation by finite differences using up-to-date 3D structural model of the Osaka basin. The strong surface waves in the region are not directly generated by these deep sources, but they originate by refraction mostly at the edges of the bedrock–sediments interface. The objective of this research is to model observed surface Love wave generated in the eastern part of the basin that propagates approximately westwards and is recorded by several surface stations. At these stations, the 3D finite-difference modeling provides a good fit with the observed surface wave in terms of waveform, amplitude, and arrival time for the most detailed 3D velocity model that contains topmost 50–250 m structure with the lowest S-wave velocities of 250 m/s. The semblance analysis of the synthetic wave field reveals that the respective synthetic surface wave is a result of interfering waves arriving in OSA and WOS stations from NE and SE directions. Performed tests reveal that such a synthetic wave field is extremely sensitive to the presence of the superficial 50–250 m thick low-velocity structure which is only a small fraction of the propagating surface wave length and occupies only part of the surface area. The ability to model the surface wave in terms of amplitude and time arrival validates the 3D structural model for long-period Osaka Bay earthquake scenario computations.

Keywords Long-period ground motions, Basin-edge generated surface waves, Low-velocity superficial layer, Finite-difference modeling, Hybrid modeling, Deep earthquake, Osaka basin

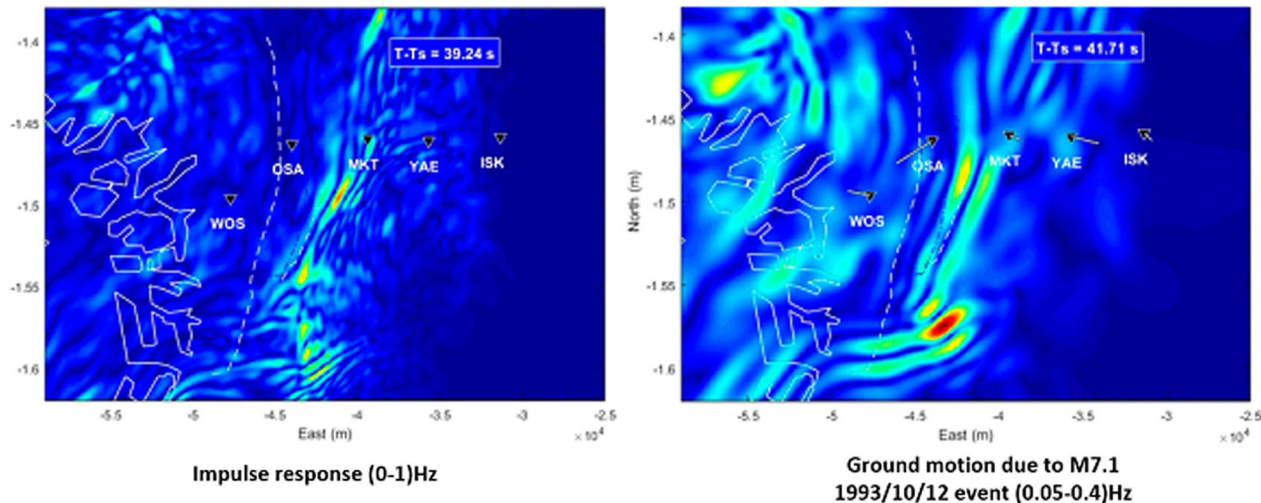
*Correspondence:

Ivo Oprsal
io@ig.cas.cz

Full list of author information is available at the end of the article

Graphical Abstract

Surface wave propagation in Osaka basin



Introduction

The importance of the long-period ground motions with long durations in earthquake hazard and risk mitigation is manifested by serious damages to large structures in period bands longer than 1 s. Such long-duration ground motions have relatively strong impact within the first few hundred kilometers of epicentral distance. They potentially affect all long-period structures (Furumura et al. 2008 and references therein) such as high-rise buildings, long bridges (Fujino and Siringoringo 2013), oil tanks (Hatayama 2008), and artificially damped structures (Ismail 2018 and references therein). For the Osaka region, the long-period motions are relevant between 1 and 10 s, namely, for shallow and large offshore events.

An important high casualty example due to seismic hazard can be well known case of Mexico City damaged at 400 km epicentral distance from Michoacán event, 1995 (Beck and Hall 1986). Among many damaging Japanese events with long-period effects, such as 2003 Tokachi-oki, Japan, earthquake (Koketsu et al. 2005; Hatayama 2008) with oil tanks damaged in the Yufutsu basin situated as far as 250 km from the epicenter—the damages reported in Tomakomai were observed on structures with eigen periods between 1.5 s and 15 s. Out of those severe damages (all in the Tomakomai west port area) were on structures with eigen periods between 7 s and 8.5 s and one case even at 12 s. Another example is the 2004 Kii peninsula earthquake (Miyake and Koketsu 2005; Iwata and Asano 2005—modeling) stimulating long-period ground motions in Omaezaki region

(Shizuoka prefecture), Kanto (with Tokyo city), Osaka, and Nobi (with Nagoya city) basins representing a wide area of Honshu, Japan, with epicentral distances from 200 to 250 km.

The Osaka metropolitan area (Fig. 1) is densely populated and threatened by earthquake hazards. The long-period ground motions modeling according to contemporary 2D or 3D Osaka basin models was done by numerous authors (Hatayama et al. 1995; Kagawa et al. 2004; Sekiguchi et al. 2008; Iwaki and Iwata 2008, 2010; Asano et al. 2016) and also the contributions to the 1998 meeting Effects of Surface Geology (Irikura et al. 1998). Yet, the studies have not concentrated on research combining the rare deep event with the temporary OSA array recording and up-to-date 3D Osaka basin model. The observations or modeling of basin-induced surface waves amplified inside the sedimentary area of basin at various locations over the world were studied by, e.g., Frankel (1993), Koketsu and Kikuchi (2000), Kawase and Aki (1989).

The focus of the present study is the interpretation of locally generated surface waves in terms of the ground motions due to deep earthquakes using up-to-date 3D velocity models of the Osaka basin. The deep 1993/12/10 $M_{JMA}=7.1$ earthquake (388 km hypocentral depth) resulted in long-period ground motions of the Osaka basin and was recorded by a relatively sparse temporal seismic network, see Table 1 and Fig. 1. Nevertheless, these recordings present a unique dataset, as there have been no strong regional deep earthquakes array

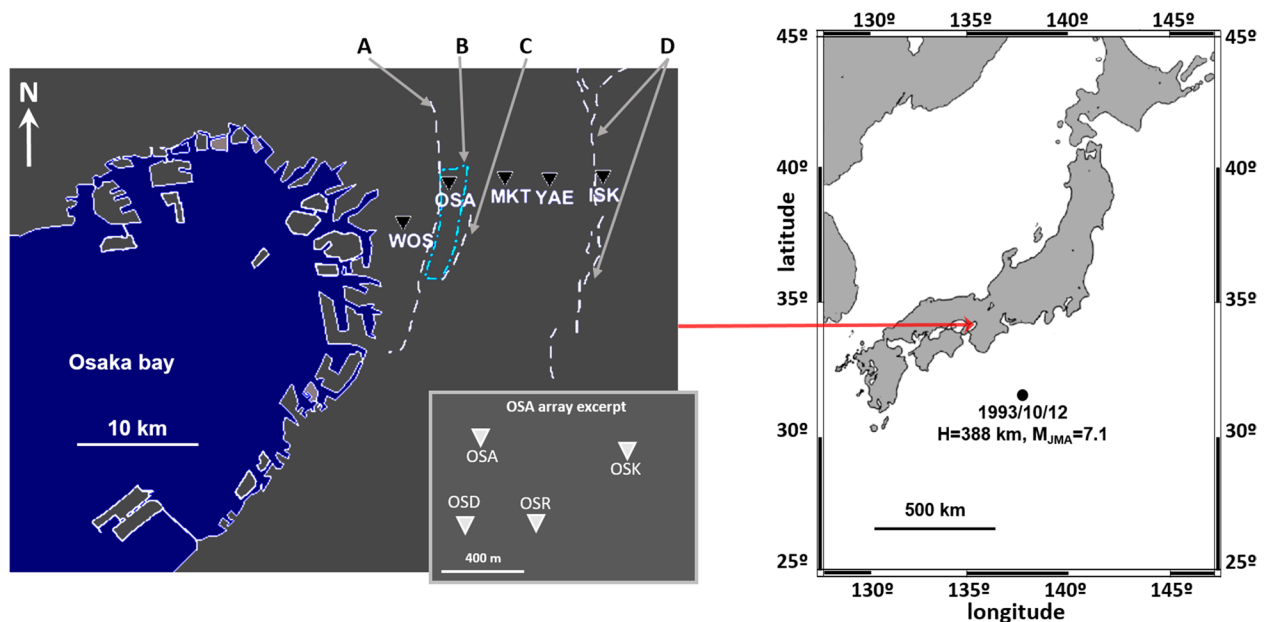


Fig. 1 Osaka bay and the October 12, 1993 event situation. The left panel shows a detail of the Osaka bay area with stations ISK, YAE, MKT, OSA, and WOS. The OSA station is one of the former four OSA array stations (OSA, OSK, OSR, OSD) with aperture approximately 400 m (see excerpt in left panel). Arrows A, C, and D point to surface traces of the Uemachi fault system, Nagai fault, and Ikoma fault system, respectively (Nakata and Imaizumi 2002). Polygon B represents the Uemachi elevation surface limits. The right panel shows the position of Osaka bay and the epicenter of the 1993/10/12 $M_{JMA} = 7.1$ event. The solid white line represents the bay shore. The positions of the stations are specified in Table 1

Table 1 Positions of the monitoring stations, the 'OSA', 'OSD', 'OSK', and 'OSR' are small-aperture array used for the semblance analysis of data. The ISK station is sedimentary near-bedrock one and can be considered a bedrock station for applied frequencies

Station name	Latitude (WGS 84) (degrees)	Longitude (WGS 84) (degrees)
'ISK'	34.68607	135.65530
'MKT'	34.68507	135.56830
'OSA'	34.68207	135.51859
'OSD'	34.67804	135.51801
'OSK'	34.68147	135.52682
'OSR'	34.67816	135.52186
'WOS'	34.65207	135.47830
'YAE'	34.68407	135.60830

recordings in the area since then. Because the hypocentral depth of the event is much larger than the surface wave eigen function reach for investigated frequencies, strong surface waves are not directly generated by this deep source. They originate as refractions mostly at the edges of the bedrock–sediments interface. Previous analysis of these recordings identified a strong long-period wave phase (called SL1), which was interpreted as Love wave locally generated at the Eastern edge of

the Osaka basin (Hatayma et al. 1995). In particular, the SL1 was generated by the S-wave impeding the eastern Osaka basin edge close to ISK station, and continuing along YAE, MKT, OSA, and WOS stations, sequentially (Fig. 1). The interpretation was based on a simplified 2D modeling of the seismic wave propagation, which could not explain the SL1 arrival time and amplitude at OSA and WOS, missing the 3D surface wave field complexity (Hatayma et al. 1995). Therefore, in the present study, we re-analyze the data with the semblance technique, as described later, and we do the same with the synthetic wave field. For this we use the up-to-date 3D velocity model of the Osaka basin and its larger locality (Sekiguchi et al. 2013, 2016). We use hybrid formulation (Oprsal et al. 2009) applied in the SW4 software 3D FD package (Petersson and Sjögreen 2017b) modified as ray-FD approach (Oprsal et al. 2002; also see Table 2) for impeding S-wave. The study can be considered as one of the validation tests of the current 3D velocity model.

The method

Finite-difference computations, hybrid formulation

The numerical simulation of the source generating seismic waves, regional wave propagation, and the local site effects is carried through by finite differences (FD). Out of presently available established seismic wave propagation codes (Chaljub et al. 2010; and references therein), we

Table 2 The effective material parameter values (Vp, Vs, density, Qp, Qs) for every FD grid layer of Vsmin250 model under the station YAE from the free surface to the upper bedrock interface (see Fig. 2, left panel)

Top depth(m)	Vp (m/s)	Vs (m/s)	Rho (kg/m ³)	Qp	Qs
0.0	1501.3	250.0	1610.5	450.4	74.7
50.0	1585.8	323.5	1717.2	475.7	97.0
100.0	1666.6	393.2	1806.9	500.0	118.0
150.0	1744.3	459.7	1883.1	523.3	137.9
200.0	1817.4	521.4	1941.8	545.2	156.4
250.0	1885.4	577.6	1980.7	565.6	173.3
300.0	1947.4	627.8	2009.2	584.2	188.3
350.0	2002.1	671.0	2030.1	600.6	201.3
400.0	2051.9	709.7	2046.8	615.6	212.9
450.0	2098.4	745.3	2061.1	629.5	223.6
500.0	2141.7	777.9	2073.6	642.5	233.4
550.0	2182.5	808.2	2084.8	654.8	242.5
600.0	2221.0	836.3	2094.9	666.3	250.9
650.0	2257.4	862.6	2104.4	677.2	258.8
700.0	2291.6	887.0	2113.1	687.5	266.1
750.0	2323.9	909.8	2121.1	697.2	272.9
800.0	2354.4	931.0	2128.5	706.3	279.3
850.0	2382.9	950.6	2135.4	714.9	285.2
900.0	2410.1	969.2	2142.0	723.0	290.8
950.0	2436.1	986.7	2148.3	730.8	296.0
1000.0	2461.5	1003.6	2154.5	738.4	301.1
1050.0	2486.7	1020.3	2160.8	746.0	306.1
1100.0	2512.0	1036.9	2167.4	753.6	311.1
1150.0	2538.2	1053.8	2174.4	761.5	316.1
1200.0	2565.0	1070.9	2181.8	769.5	321.3
1250.0	2592.4	1088.3	2189.5	777.7	326.5
1300.0	2620.3	1105.8	2197.5	786.1	331.7
1350.0	2648.6	1123.3	2205.6	794.6	337.0
1400.0	2676.4	1140.3	2213.7	802.9	342.1
1450.0	2696.4	1152.4	2219.7	810.7	346.4
1500.0	2727.2	1171.0	2228.5	818.2	351.3
1550.0	3093.2	1436.4	2275.3	825.8	360.3
1600.0	3668.2	1857.4	2343.8	832.5	370.5
1650.0	4131.7	2196.3	2399.5	837.6	378.9
1700.0	4591.2	2532.9	2454.1	841.5	386.5
1750.0	5160.1	2950.3	2520.5	844.6	395.1
1800.0	5500.0	3200.0	2560.0	846.2	400.0
1850.0	5500.0	3200.0	2560.0	846.2	400.0

use the freely available SW4 (Seismic Waves, 4th order) code of Petersson and Sjögreen (2012; 2015; 2017a,b). After careful consideration, the SW4 code appears to be optimal in time efficient for in the computer-demanding Osaka basin wave propagation simulations. The code can simulate seismic wave generation and propagation

in a topographic 3D inhomogeneous viscoelastic anisotropic medium. Its design enables a distributed-memory parallel run. The governing viscoelastic equations are approximated by fourth order of accuracy in space using a grid-node-based finite-difference approach and by explicit time formulation. The SW4 may apply a curvilinear grid to incorporate curved topography, local vertical mesh refinement to cover well computation of high elastic moduli areas inside the hard rock and very low moduli in the soft sediments at the same model. The method is stable for high Poisson's ratios and high Poisson's ratio contrasts and allows for a realistic model of seismic attenuation. The auto-generated meshing is based on specific numerical requirements.

The parallel computations presented in this study are required to be accurate in the period range of 1 – 100 s with the lowest S-wave velocities 250 m/s located in the superficial parts of the model. The size of the complete all-in-one computational FD model, including the 388 km deep source with epicentral distance around 380 km, would be rather large. Because of the computer-time and memory requirements of such settings for complete P- and S-wave filed included in one computation, we consider only the S-wave impeding the Osaka basin in a two-step hybrid formulation (Oprsal et al. 2009) in hybrid ray-FD variant (Oprsal et al. 2002; and see Appendix 1). In the first step, the ray method for source and path effects up to regional structure is considered. Following second step is using local FD with Osaka basin structural model included. The second-step results then contain source, path, and site effects for the S-wave part of the wave field impeding to the basin.

The code has been thoroughly tested and validated against analytical and numerical methods (Petersson and Sjögreen 2017a; and references therein), while the hybrid formulation adopted inside SW4 was tested against full-scale computation by the SW4 by replication tests generalized by Oprsal et al. (2009).

Geological structure and FD computational model approximation

There have been many geological and geophysical techniques extensively investigating the 3D Osaka basin structure on various size scales and locations over the past decades (e.g., Horikawa et al. 2003; Kagawa et al. 2004; Iwata et al. 2008; Iwaki and Iwata 2011). We use the most up-to-date 3D Osaka velocity structure model (Sekiguchi et al. 2016) with recent updates (Iwata and Sekiguchi, pers. comm. 2021). The size of the presently used Osaka basin area geological model is 85 km × 90 km, respectively (left panel of Fig. 2). As to the depth, the lowest layer crustal interface between 30.86 km and 34.58 km is modified to be horizontal at

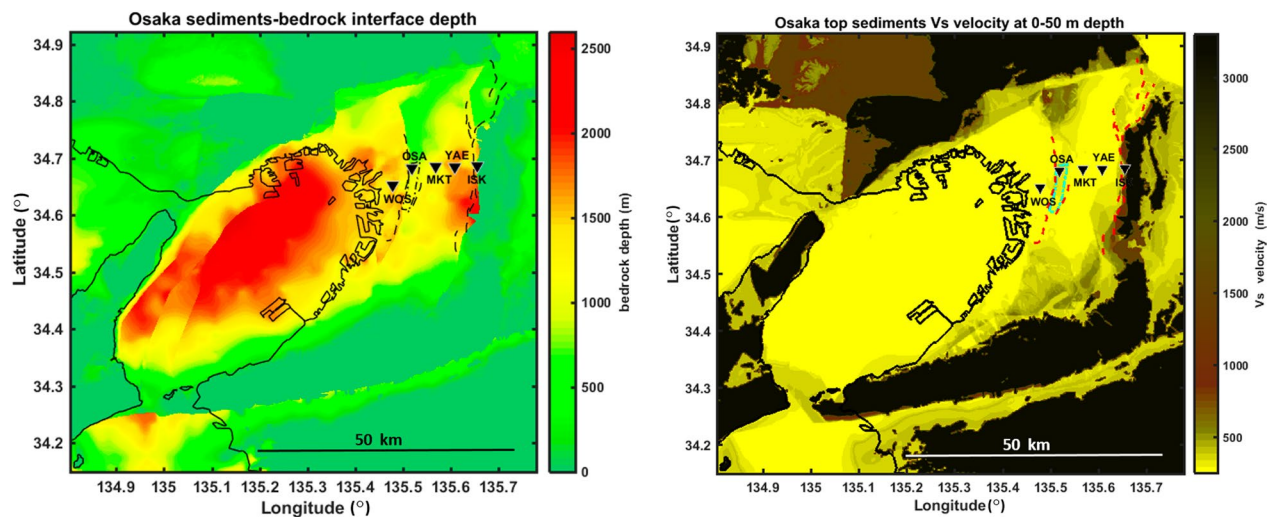


Fig. 2 Left: Osaka basin geological model—bedrock depth (SN x WE = 85 km x 90 km). Right: Computational Vsmin250 model Vs velocity of the 0—50 m depth. See Fig. 10 in Appendix for further depths' details

a 32 km depth. Deeper structure is adopted from the PREM isotropic model (Dziewonski and Anderson 1981), as non-decreasing function (Bormann 2012, Datasheet DS 2.1, Table 1).

In order to represent the 3D continuous velocity model in SW4 properly, it is transformed into FD computational grid of effective parameters with a grid step of 50 m following the procedure shown in Oprsal and Zahradnik (2002, par. 2.5.3). The detailed velocity model (Fig. 2) is completely included in terms of horizontal dimensions and goes approximately to a depth of 2.7 km. The size of the computational model is further enlarged to NS x EW x DEPTH = 118 km x 123 km x 3.1 km by adding the non-reflecting boundaries. The lowest S-wave velocity in the superficial parts of the model (Sekiguchi et al. 2016) is 248 m/s. It serves as input for computational model with finest gridding of 50 m. The lowest S-wave velocity of the computational model is 250 m/s. For the numerical experiments, we also consider another model with minimum S-wave velocity $V_s = 500$ m/s for each computational cell with original $V_s < 500$ m/s. Hatayama et al. (1995) used the 500 m/s superficial layer to improve the arrival time and amplitude of the SL1 fit. Moreover, it allows to show dependence of the results on the superficial layers' velocity. These models are hereinafter called Vsmin250 and Vsmin500, respectively. The topography is flat and no water medium is considered. The topography and sea-bottom upper structure is shifted into flat topography while keeping the upper-basin structure vertical profile under each such FD horizontal surface point unchanged according to original topographical model vertical profile. The Q_p and Q_s are realized by viscoelastic modeling using three standard

linear solid mechanisms (Petersson and Sjögreen 2012; 2017a) providing correct damping for periods of 0.4 – 40 s.

The seismic source

The $M_{JMA} 7.1$ event of October 12, 1993 was the only strong deep regional event recorded during temporary operation of the OSA array, while also recorded at ISK, YAE, MKT, and WOS stations (Hatayama et al. 1995). The point source located at Lat = 32.017N, Lon = 138.233E, depth = 388 km (after Hatayama et al. 1995) is represented by a double couple of [strike, dip, rake] = [171, 82, 81] degrees (JMA nodal plane solution, referred to as 1993/10/11 15:54:20.90 event, ID447083). The generated waves are propagated by ray method in 1D layered medium in the first hybrid step. We compute only S-wave ray from source up to the excitation box boundary underlying the whole Osaka basin computational area. The time history of the ray-propagated S-wave pulse is integrated Ricker wavelet with $\omega = 0.50$ Hz (Petersson and Sjögreen 2017a). To represent the complexity of the source function, the complete 3D FD hybrid response is then convolved with EW horizontal component of near-bedrock ISK station recording of the 1993/10/12 $M_{JMA} = 7.1$ event. The simulated results (and data) are band passed between 0.05 and 0.4 Hz. The applied band encompasses the frequency range where the observations match the dispersion curve of the fundamental mode of the Love wave, which is the main feature of SL1 (Hatayama et al. 1995).

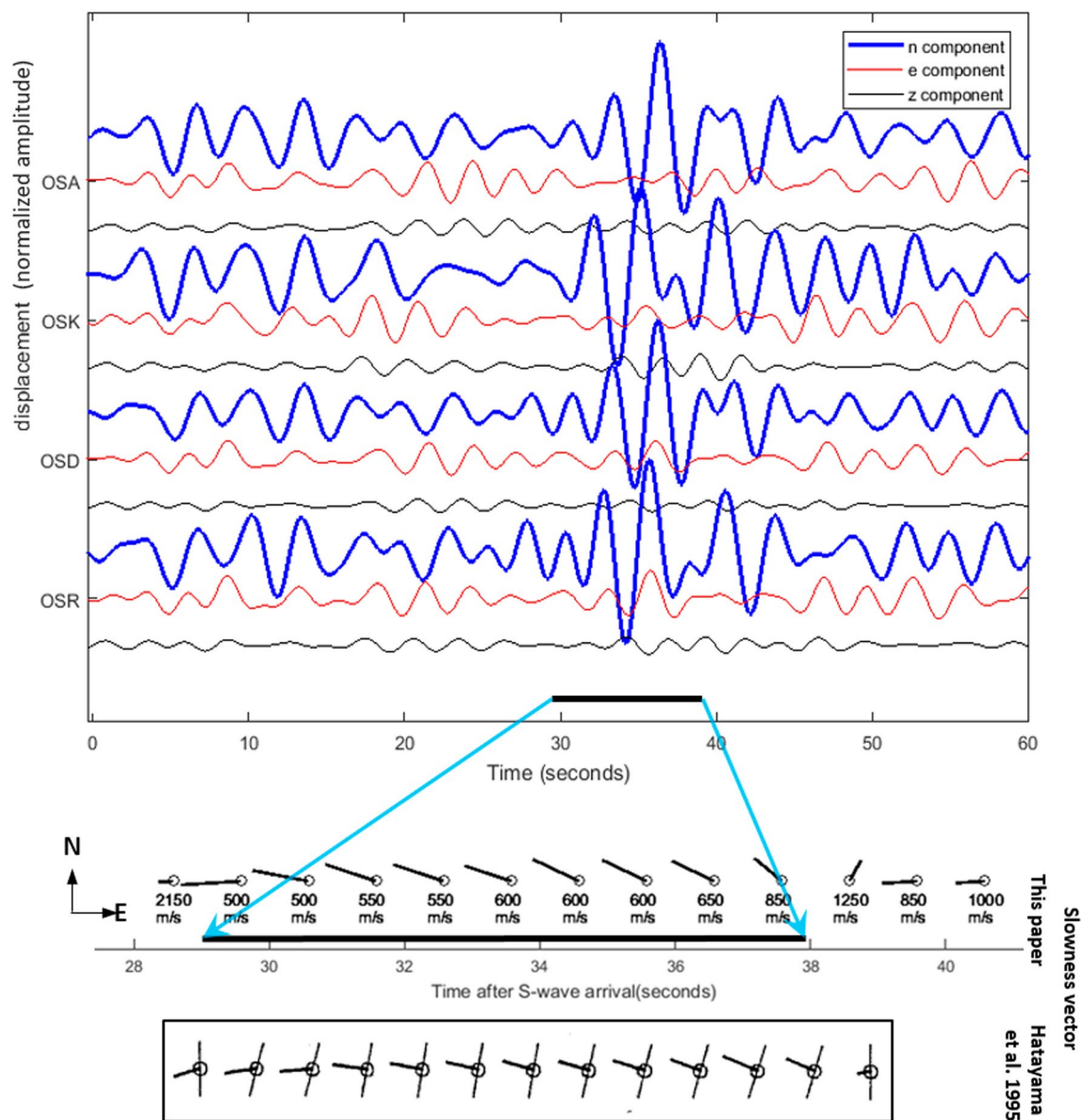


Fig. 3 The data recorded at the OSA array (upper panel) for the 1993/12/10 $M_{JMA} = 7.1$ event. The aperture of the array is approximately 400 m (see Table 1 and Fig. 1). The data are band passed between 0.2 and 0.38 Hz for the semblance analysis (Hatayama et al. 1995). The lower panel shows semblance analysis of time dependence of the apparent slowness vector inferred from the horizontal ground motion for times between 29 and 38 s after the S-wave arrival. For each time point, the stick length means wave propagation slowness, its direction shows the prevailing wave propagation direction in the horizontal plane, and the number corresponds to the propagation velocity. The horizontal axis in both panels is time after the incident S-wave arrival, thick horizontal line in both panels depicts the presence of low-velocity wave, presumably the SL1. The lowest panel is resulting semblance analysis for the same data by Hatayama et al. (1995) showing slowness and polarization directions, see Ibid for further analysis of the data. This experiment serves as a consistency test for the implementation of the semblance technique

Semblance and polarization analysis

We adopt the semblance technique (Neidell and Taner 1971) to determine the apparent wave propagation velocity and direction at a given point and time, see Fig. 3. It is applied to band-passed time histories of a respective array. The frequency range that we utilize for the

semblance calculation is from 0.20 to 0.38 Hz. This range is specifically chosen because it encompasses the frequency band where the energy is the strongest (Hatayama et al. 1995). Additionally, narrowing the frequency band for this particular analysis also helps stabilize the results. The necessary time window for each semblance

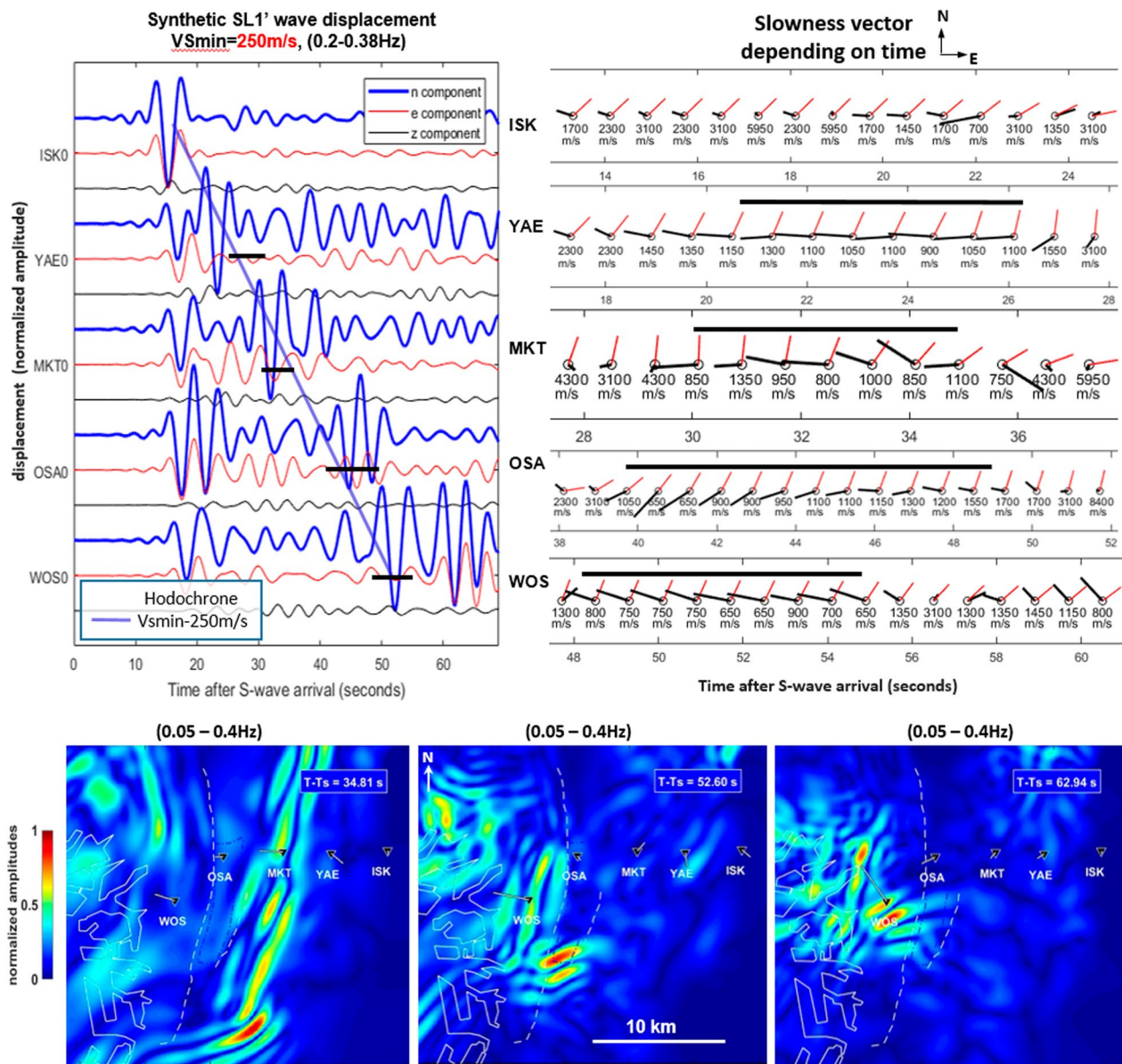


Fig. 4 Surface wave propagation – semblance analysis. The left upper panel shows the band-passed synthetics (0.2–0.38 Hz) used for the semblance for model $V_{\min}250$ at particular station of arrays ISK, YAE, MKT, OSA, and WOS. The black bar shows identified SL1' surface wave. The right panel shows the time series of the slowness vectors (in black) with detected slowness in m/s (from semblance technique). The corresponding polarization azimuths are represented by the red sticks. The bottom panels are snapshots of total horizontal component of the simulated wave field (0.05–0.4 Hz). The SL1' surface wave arriving at MKT (~ 34.8 s, left bottom panel) and at WOS (~ 52.6 s, mid bottom panel) is succeeded by another surface waves group. That results in change of apparent wave propagation direction from WNW to NNW at WOS at about 57 s when (after 58 s) it depicts a wave group propagating in the NNW direction. The lines originating at each of the stations show apparent slowness vector at respective times

central time, determined by the frequency content of the narrow-band signal, is 1.9 s; hence, the semblance sensitivity (or uncertainty) in time is approximately 1 s. The semblance value threshold is specified in the results. The FD synthetics are analyzed for respective arrays placed at location of each of the five stations (ISK, YAE, MKT,

OSA, and WOS); the aperture of each such virtual array is 400 m.

The time–frequency polarization analysis is then used to characterize particle motion at a given point. This motion is, in general, elliptical for a short time window

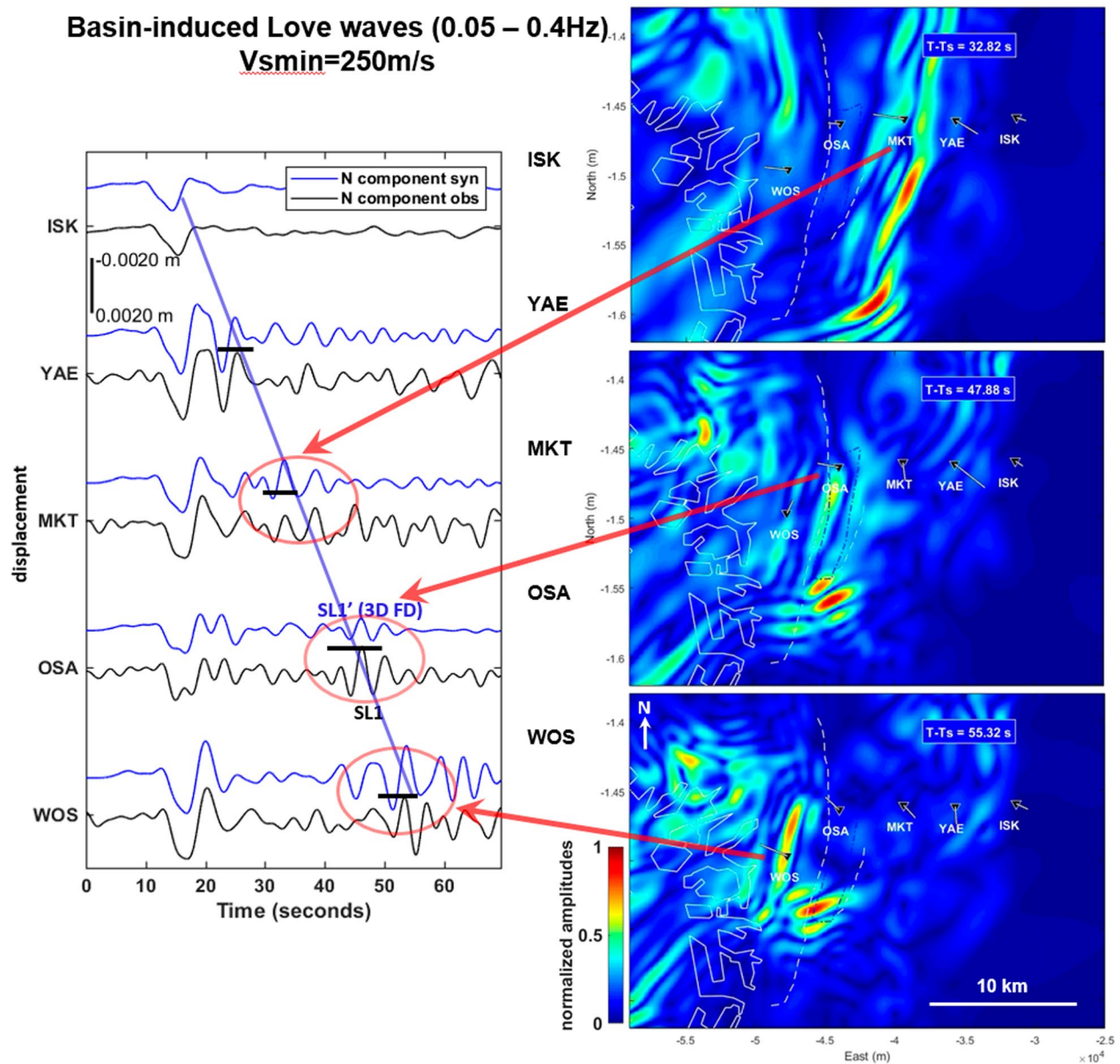


Fig. 5 Left panel compares the synthetics (model V_{s250}) to data 0.05–0.4 Hz. The black bars identify SL1' phase (red circles) identified by semblance in synthetics. The blue line is approximate SL1' hodochrone. The right panels are snapshots (0.05–0.4 Hz) for respective SL1' arrival times at MKT, OSA, and WOS. The sticks at the snapshot stations are slowness vectors

and is described by the orientation of the semi-major axis of the ellipse in space (Burjánek et al. 2010).

Results

The presumed surface wave generated in the bedrock-basin border in the vicinity of the ISK station due to incident S-wave and structural discontinuity close to Ikoma fault propagates along the free surface approximately in the WNW direction. The semblance analysis for station locations ISK, YAE, MKT, OSA, and WOS are shown

in Fig. 4, upper right panel. The value of the semblance threshold is 0.80. The minimum observed semblance values ($SB_{station_name}$) for the Love-wave arrivals are as follows: $SB_{YAE} > 0.85$ (typically 0.90), $SB_{MKY} > 0.88$ (typically 0.90), $SB_{OSA} > 0.9$ (typically 0.95), and $SB_{WOS} > 0.93$. Figure 4 shows apparent slowness and polarization vectors of the horizontal ground motion at distinct times to indicate the presence, direction, and apparent velocity of the surface Love wave (mostly visible on NS component, i.e., transverse direction to slowness vector). The

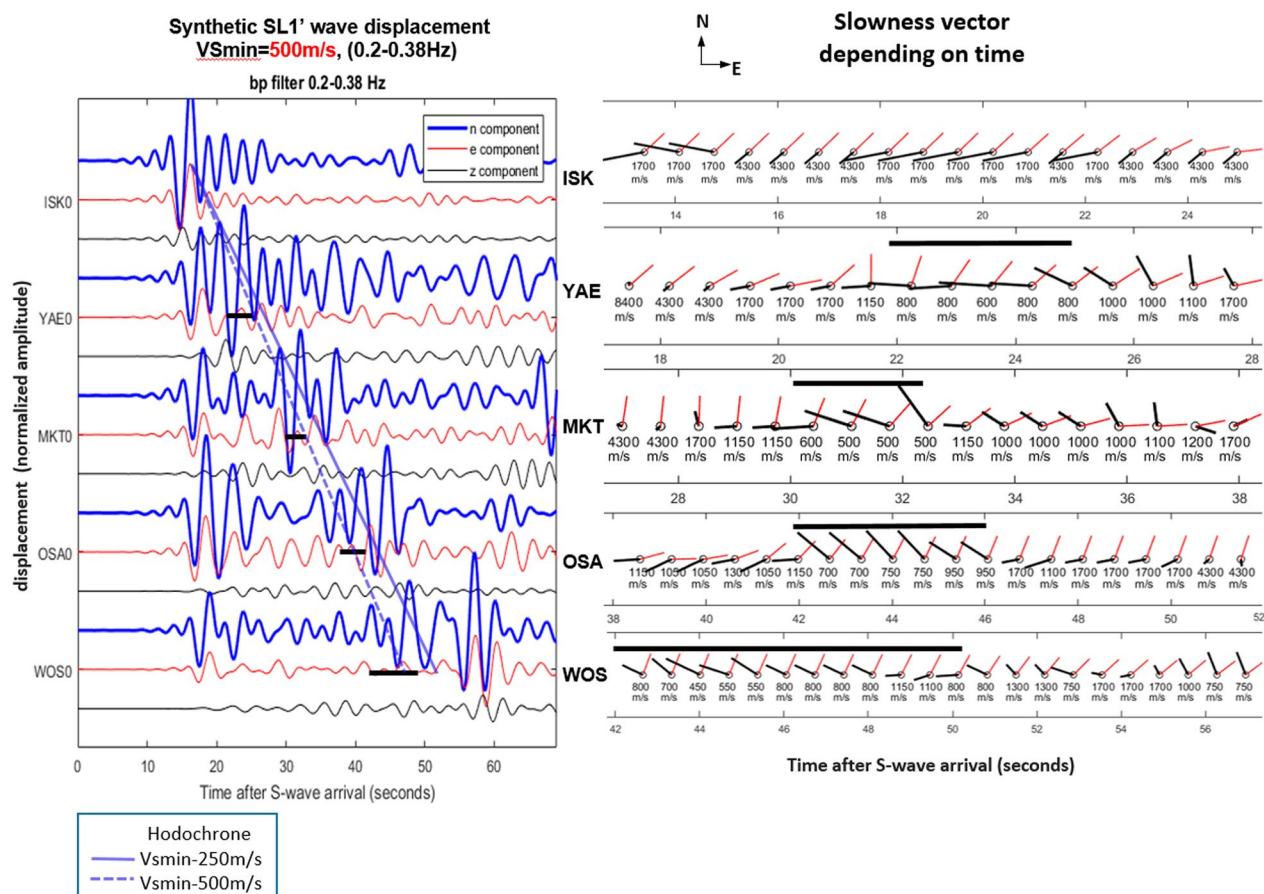


Fig. 6 Surface wave propagation – semblance analysis. Left upper panel: The synthetics band passed for the semblance analysis (0.2–0.38 Hz) for model $V_{sm}=500$ m/s at a particular station of each of the FD arrays used for semblance analysis. The right panel shows the time series of the slowness vectors (in black) with detected slowness in m/s (from semblance technique). The corresponding polarization azimuths are represented by the red sticks. See also Fig. 4

velocity of the surface Love wave, present between times of 39 and 41 s, is mostly between 650 and 800 m/s being slightly higher than for the data, heading SW and turning to WNW after 5 s with velocity between 1000 and 1500 m/s, which is mainly due to the reason that two wave groups are arriving at the OSA station at a similar time. This is also manifested by inconsistent polarization azimuth with respect to obtained slowness vector. The animation and respective snapshots suggest that the surface waves were created at the eastern edge of the Osaka basin, contoured by the Ikoma fault system (Figs. 1, 2), and were directed differently due to the curved shape of the basin edge and the 3D structure in the area. Figure 4 shows the semblance analysis also for YAE, MKT, and WOS with the Love-wave velocities are between 650 and 1000 m/s. Prevailing propagation at YAE and MKT is in a westward direction, while at WOS the wave propagates toward a WNW direction. The synthetics are shown for stations and arrays corresponding to their real positions.

The synthetic solution shows relatively strong and long-lasting oscillations at OSA station; however, the longer wave train does not really correspond to sole SL1' surface Love wave as depicted in Fig. 4. The amplitude of the SL1' wave is stronger also at the WOS station, with short duration and little earlier arrival than the observed SL1. For semblance analysis of data recorded at OSA array see Fig. 3. The comparison of the synthetic to data is shown in Fig. 5. The timing and fit of the impending S-wave synthetics and data are very good in terms of timing and amplitudes at ISK station, and the OSA data are more oscillatory than synthetics. Arrival of SL1' at all stations is satisfactory enough to visually correlate the same SL1 on data for YAE, MKT, and WOS. The amplitudes at OSA station are a bit lower in the synthetics. Later arrivals (after 59 s) at WOS belong to another wave group arriving from SES (see also Fig. 4) that is generated at the basin edge located approximately 25 km SES of the WOS

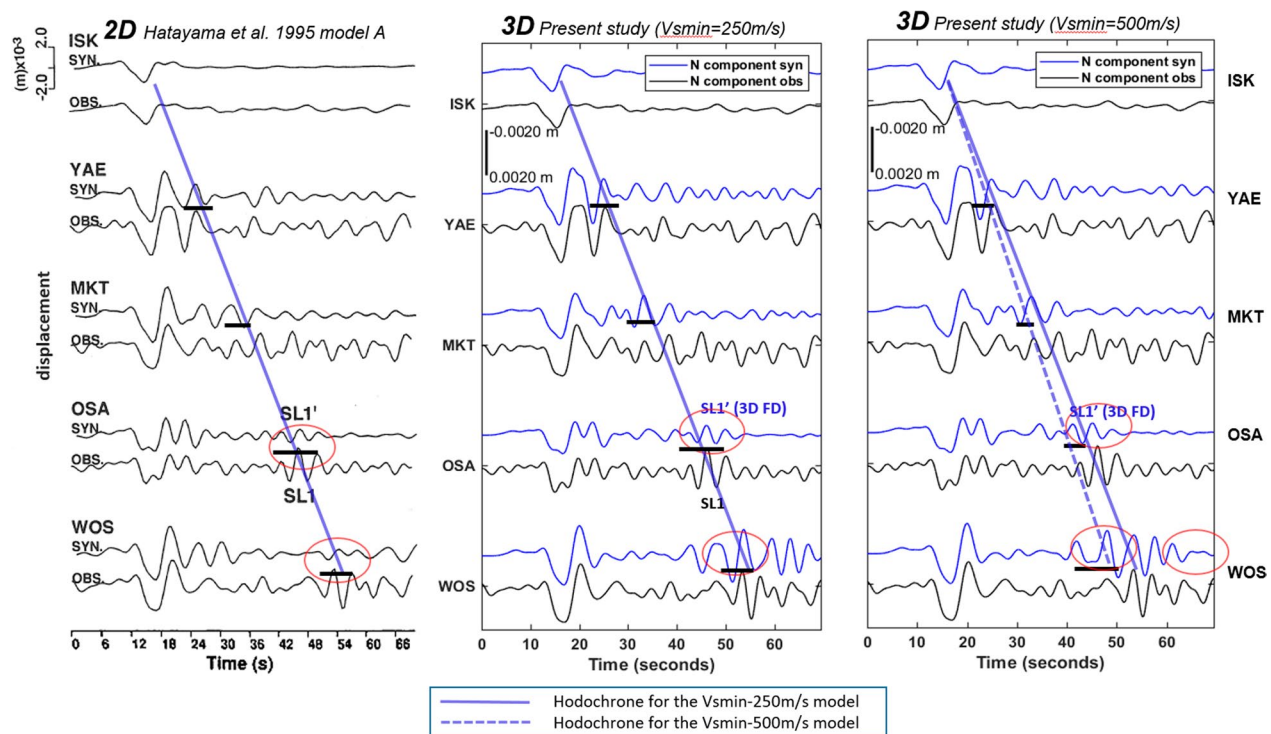


Fig. 7 Comparison between synthetics and data at five stations depicted in Fig. 1, NS component of displacement. Left panel is modified from Hatayama et al. (1995). Comparison for the given (1993/10/12 $M_{JMA}7.1$) event and synthetics for 3D geological model (Sekiguchi et al 2013, 2016) modified as $V_{min}250$ (mid panel) and $V_{min}500$ (right panel). The data and synthetics are band passed within 0.05–0.4 Hz. The model with low velocities ($V_{min}250$) preserves the SL1' phase in OSA and WOS stations, and the shift of SL1' surface wave hodochrone for stations further from ISK is due to higher average surface wave velocity

station (see attached full-scale animation, Figs. 1, 2, and 12).

We have done an additional numerical experiment for the same setting with modified 3D FD model called $V_{min}500$ (Fig. 6) to approximate modeling cases of previous research of Hatayama et al. (1995) who added a superficial layer of 500 m/s to the model to emphasize the surface wave velocities and to add some oscillatory part to the wave field. On the other hand, this model is simpler and “faster” in the vicinity of the free surface sedimentary parts of the Osaka basin, than the $V_{min}250$ model. As a result of the higher propagation velocities and lower attenuation, the single-top-layered $V_{min}500$ model results are showing a different SL1' hodochrone (read from waveforms) and are less complex. The slowness vector has changed direction from WNW to NNW at WOS at about 54 s compared to $V_{min}250$ case. OSA station shows predominantly NW-propagating surface wave of 700 m/s at 44 s contrary to the same case in $V_{min}250$, where it propagates in SW direction at 46–50 s at 1100 m/s with much more complex arriving wave field. The difference of the SL1' phase apparent velocity and propagation direction is substantial. Because the semblance technique is able to pick only one apparent

slowness or velocity vector at a time, its sensitivity in this case indicates relatively high sensitivity of the wave field amplitudes and directions on the superficial part of the model in terms of generation of the surface waves, their amplitudes, and propagation.

Comparison of the best solution of the 2D FD modeling (Hatayama et al. 1995), the V_{s250} and the V_{s500} 3D FD modeling are then shown in Fig. 7. Basin-induced Love waves SL1 are compared at the five stations. The model with low velocities ($V_{min}250$) preserves the SL1' phase in OSA and WOS stations. The $V_{min}250$ and $V_{min}500$ model results do not differ much in the earliest times after the S-wave arrival thanks to prevailing low-frequency content of the signal. The differences of the hodochrone in $V_{min}250$ and $V_{min}500$ solutions is due to slightly different average group velocity of the SL1' phase for different models.

Conclusions

The wave propagation in the Osaka basin, including the surface waves, is essentially a 3D wave propagation problem. The low-period S-wave of the respective event with simple pulse-like character generates surface waves at the eastern and south-eastern edges of the model. The

waves propagate throughout laterally inhomogeneous Osaka basin structure, where they mutually interfere. The 2D numerical modeling of the case does not provide the complexity of the surface wave field, where the structural complexity trades off the amplitudes with arrival times.

In 3D modeling, we have used the up-to-date 3D structural model of the Osaka basin called Vsmin250. Added to that we also tested its modification called Vsmin500 to reflect the fact that the 2D modeling of SL1' Love surface waves had improved only partially in time arrivals without a good amplitude fit by adding the superficial Vs = 500 m/s layer of 400 m thickness atop of the basin (Hatayama et al. 1995). Both of the two 3D models have local superficial strata of various thickness and minimum Vs being 250 and 500 m/s, respectively, the latter simplifying heterogeneous near-surface velocity structure.

The thin low-velocity parts of the model are important even in low-frequency bands. Counter-intuitively, the superficial 50 m thick low S-wave velocity areas occupying only 1/20 to 1/10 of S-wave length are reasonably influencing the wave field in terms of surface wave propagation. It is due to the fact that the respective wave spends several periods when traveling through such a thin low-velocity stratum patch of the surface. Thus, the propagation of strong Love waves inside the basin is conditioned by presence of near-surface low-velocity structure, or as an approximation, by thin low-velocity structure of 50–200 m thickness which is a small fraction of the S-wave length.

The 3D FD modeling validates present 3D Osaka basin structural model (Vsmin250) by the synthetic SL1' phase generated at the Eastern part of the Osaka basin. This wave exists for both structural models with Vsmin = 250 m/s and Vsmin = 500 m/s. A near-surface layer being fraction of wavelength thick reasonably influences the wave field in terms of prevailing surface waves. The amplitude of the SL1' phase depends strongly on the azimuth of the impeding S-wave. Therefore, the present computational 3D velocity model Vsmin250 prepared within this study (based on Asano et al. 2016) is suitable for long-period Osaka Bay earthquake scenario computations.

Wave propagation in both 3D models, Vsmin250 and Vsmin500, contains the SL1' phase in OSA and WOS stations in low-frequency band. Vsmin500 model SL1' has earlier arrivals and lower amplitudes in further stations (OSA and WOS).

The differences in semblance result for Vsmin250 and Vsmin500 model synthetics (in band 0.2–0.38 Hz) are caused by scattered wave field arrivals at higher frequencies contained in the Vsmin500 model arriving from different directions. The semblance analysis for the OSA array shows Love wave propagating mostly in NWN

to SWS directions for data and for both FD synthetic models. The reason for earlier synthetic Love-wave arrival at WOS station may be that the computational model's lowest S-wave velocity was kept above 500 m/s limit. This clearly manifests strong sensitivity of the long-period wave field to the presence of small volumes of low propagation velocities in the 3D model.

Modeled 3D wave field at OSA station at the time of SL1' phase arrival is a mixture of several surface waves traveling in SWW and WNW directions, while the semblance technique picks only one of the directions from the whole arriving surface wave field. This suggests that the real observed SL1 surface wave phase is not generated solely at the eastern edge of the Osaka basin and does not arrive at the stations purely from an EW direction. The simulations support the possibility that these surface waves traveling in different directions come across at OSA at the time of SL1. There is high possibility that both are generated along Ikoma fault system (eastern edge of the Osaka basin) propagating in slightly different directions because of the bent shape of the basin edge line and 3D structure between the basin edge and OSA.

Appendix 1

The hybrid box technique can inject wave field containing source and path effects inside local or regional FD hybrid model while being permeable for any wave field – scattered inside the box or backscattered into the box from outside. The following shows the hybrid method (Oprsal et al. 2009) applied for case of planar S-wave traveling arbitrarily from below with purely horizontal displacements, which is strongly simplifying the Eq. 22 (Ibid) to be used in the following example. The hybrid box is realized by horizontal double FD plane throughout the whole model. Horizontal forces added to the elastodynamic equation at neighboring FD points (as in Fig. 8) of the box realize the traction discontinuity. The application of sole forces assures permeability of the box.

Let $u_{FD1}(t_{ray})$ and $u_{FD2}(t_{ray})$ be time-integrated histories of displacements computed by ray method in a certain point, where t_{ray} is time of the histories (Fig. 8). Let further t_{FD} be the time history in the FD method and time shift,

$$t_{ray} - t_{FD} = t_{sh}, \quad (1)$$

be a constant shift, which is a usual case when FD computation starts at $t_{FD} = 0$ while t_{ray} reflects the travel time from source. For brevity of the demonstration, let us consider only horizontal-motion planar S-wave. Then the time history of, e.g., horizontal forces (for SW4 method)

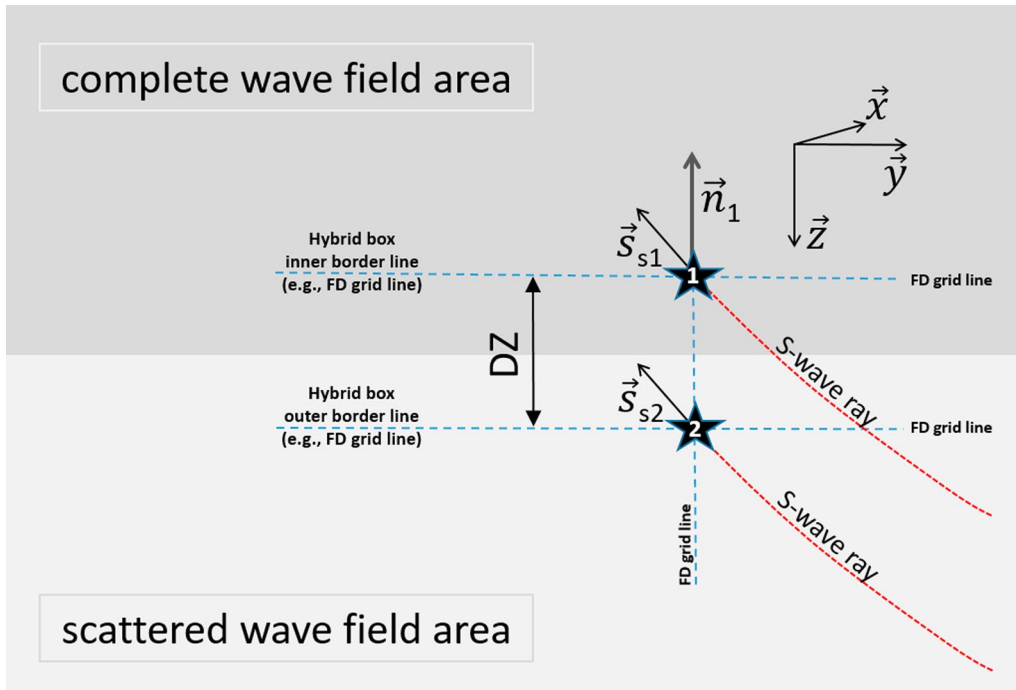


Fig. 8 2D section of the hybrid FD method second-step realization of the incident S-wave. Voluminal horizontal forces are applied at discrete sources placed at neighboring FD grid points—stars 1 and 2 belonging to the complete and scattered wave field, respectively. The scattered wave field is zero for replication test (see Figure 9) The excitation wave field bounding of the first step is pre-computed by the ray method; the second hybrid FD step is either the simple ray model structure (for replication test) or the Osaka basin structure. The inner and outer border lines placed at grid lines (on grid planes in 3D) are possible finite-extent realizations of the hybrid boundary. Vectors \vec{s}_1 and \vec{s}_2 are S-wave slowness vectors, \vec{n}_1 is normal vector to the horizontal grid plane

prescribed at FD grid point 1 (scattered wave field area, Fig. 8) is

$$f_{FD1}(t_{FD}) = \frac{\mu}{DZ} u_{FD1}(t_{ray} - t_{sh}), \quad (2)$$

and the time history of, e.g., horizontal forces prescribed at FD grid point 2 (scattered wave field area, Fig. 8) is

$$\begin{aligned} f_{FD2}(t_{FD}) &= f_{FD2}(t_{ray} - t_{sh}) \\ &= -\frac{\mu}{DZ} u_{FD2}(t_{FD} + \vec{s}_2 \cdot \vec{n}_2 DZ) \\ &= -\frac{\mu}{DZ} u_{FD2}\left(t_{FD} + \frac{\vec{s}_2}{|\vec{s}_2|} \cdot \vec{n}_2 \frac{DZ}{v_s}\right), \end{aligned} \quad (3)$$

where μ is Lamé's parameter, v_s is the S-wave velocity, and other variables are depicted in Fig. 8, $\vec{s}_1 = \vec{s}_2$ for planar wave, thus having the FD point 1 ray method wave field values sign-reversed and being delayed by $\vec{s}_2 \cdot \vec{n}_2 DZ$ to be applied in FD point 2. In this case, the first-step ray (paraxial) computation f_{FD2} can be expressed as

$$f_{FD2} = -f_{FD1}(t + \vec{s}_1 \cdot \vec{n}_1 DZ). \quad (4)$$

The same result could be obtained using the wave equation. For incident planar wave impeding vertically (4) simplifies further to

$$f_{FD2vert}(t_{FD}) = -f_{FD1vert}(t_{FD} + \vec{s}_2 DZ) = -f_{FD1vert}\left(t_{FD} + \frac{DZ}{v_s}\right). \quad (5)$$

Hence, paradoxically, the prescribed force realized at the scattered-wavefield nodal point 2 is delayed by $\frac{DZ}{v_s}$ and has the opposite sign to the force realized at the complete-wavefield nodal point 1 (Fig. 8). The opposite signs of the f_{FD} force are finite-difference realizations of (point) traction discontinuity $f_{FD2} - f_{FD1}$ on the permeable hybrid boundary. Thus, general traction discontinuity realized by voluminal forces $f_{FD2} - f_{FD1} = f(u_{FD})$, where u_{FD} is displacement at the hybrid boundary computed in the first step (here by the ray method). Both, u_{FD1} and u_{FD2} , have to be computed to approximate ∇u_{FD} and $\nabla \cdot u_{FD}$ in the Eq. 22 and paragraph 2.5.1 of Oprsal et al. (2009). The mentioned Eq. 22 also shows that applying u_{FD1} and u_{FD2} as described in the above example produces time wave field being derivative of the impeding u_{FD1} at the inner boundary. In the SW4 code, the voluminal force discontinuity is realized, as FD approximation,

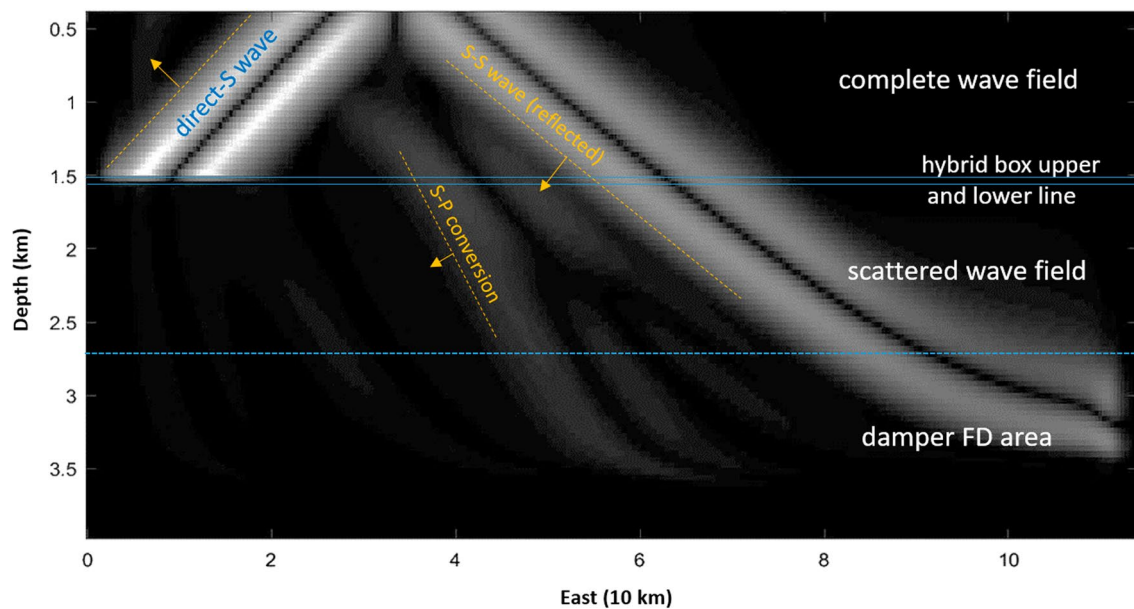


Fig. 9 Hybrid method second step: replication test of the Ricker pulse S-wave. Snapshot at the edge of the computational model. Total horizontal component of velocity at vertical section of the second-step hybrid model at depth of 400 m to 4000 m (free surface not shown). The arrows are slownesses (not to scale). The S–S reflected wave propagates through the hybrid box because it is not contained in the incoming (background) wave field. Should the S–S be included in such background wave field, the SS reflection would be perfectly absorbed by the hybrid box; hence, it would be present only in the complete wave field part in the second hybrid step (as described in Oprsal et al. 2002 for DWN-FD and ray-FD hybrid formulations)

in every two grid points (upper and lower) of two neighboring horizontal grid planes placed under the whole regional computational model including the damping area. The amplitudes of the forces are tapered to zero within the damping area at the edges, where the upper and lower hybrid box planes go through. Hence, there are

no sides to the box in this case. There are around 180 000 automatically generated single-force point forces (or 90 000 traction discontinuity dipoles) with negligible influence on computational speed. The point forces are being active from 7 to 25 s of FD computation time history corresponding to complete coverage of the area by the

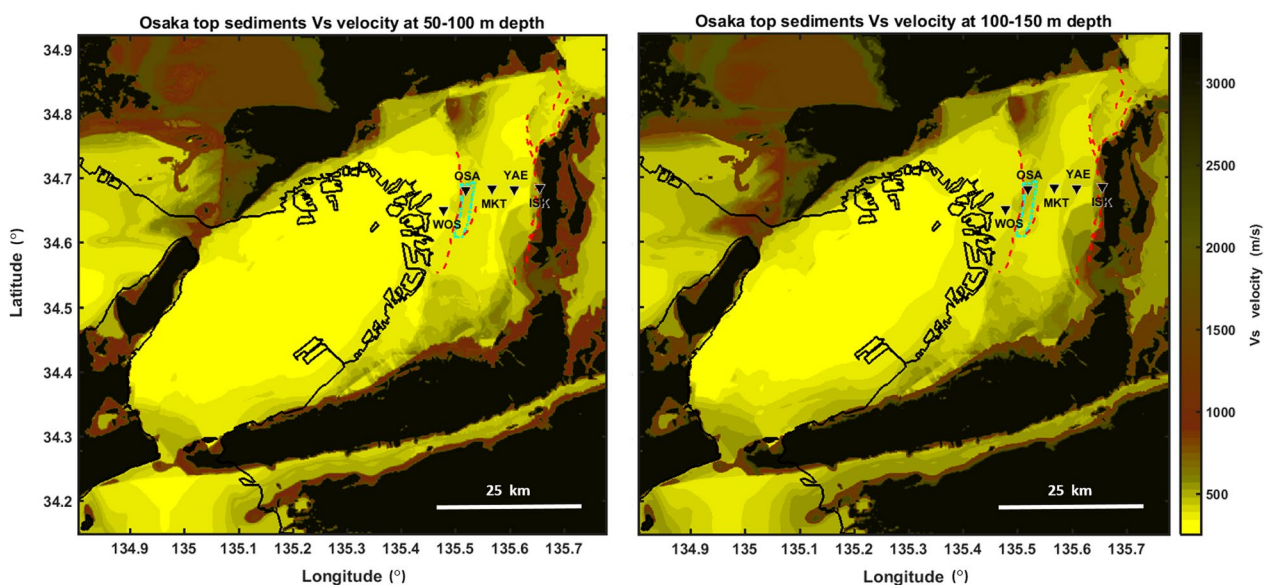


Fig. 10 Computational Vsmin250 model Vs velocity of the 50–100 m and 100–150 m depths

obliquely impeding S-wave. Complete ASCII SW4 input for parametric forces is less than 18 MB of data in our case.

Appendix 2

Computational Vsmin250 model Vs velocity of the 50–100 m and 100–150 m depths is shown in Fig. 10.

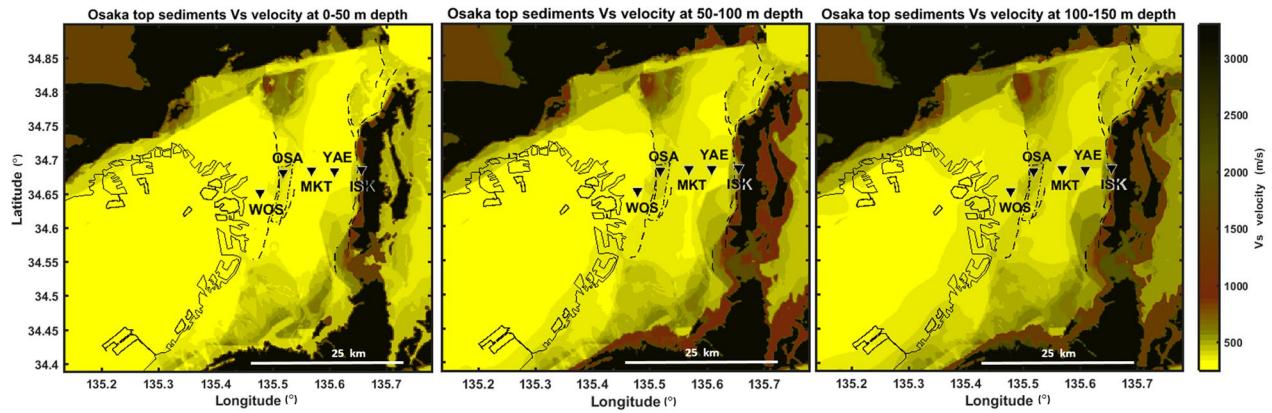


Fig. 11 Excerpt of the computational Vsmin250 model Vs velocity of the 50–100 m and 100–150 m depths

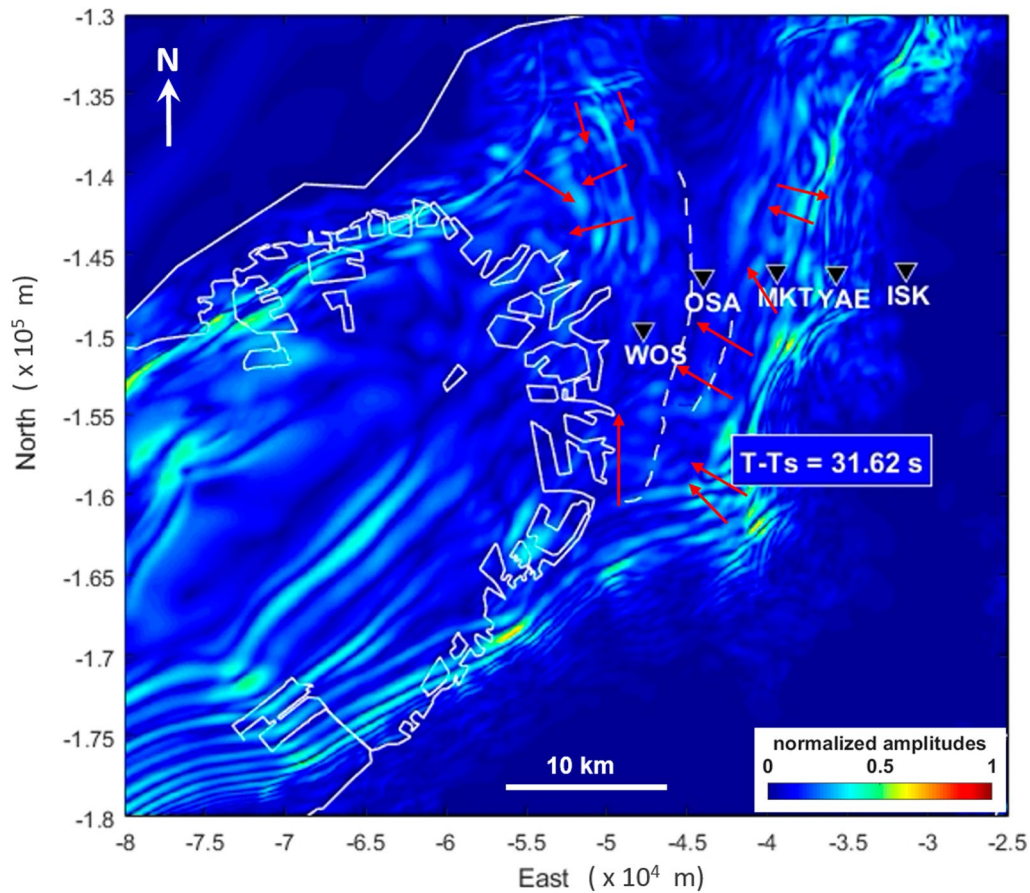


Fig. 12 The snapshot of horizontal ground motion illustrating the complexity of the scattered wave field of the Osaka basin's response in the frequency range of 0–1 Hz to the 1993/10/12 $M_{JMA}7.1$ event. The red arrows indicate the propagation of surface waves in the eastern part of the Osaka basin

Excerpt of the computational Vsmin250 model Vs velocity of the 50–100 m and 100–150 m depths is presented in Fig. 11.

Horizontal ground motion at band 0–1 Hz. The red arrows show propagating surface waves in the eastern Osaka basin is shown in Fig. 12.

Abbreviations

3D	Three dimensional
FD	Finite difference/ finite differences
SL1	Surface Love wave (data)
SL1'	Surface Love wave (synthetics)
M _{JMA}	Magnitude by Japan Meteorological Agency
NS	North–south (a direction parallel with lines of longitude)
EW	East–west (a direction parallel with lines of latitude)
NW	Northwest
SW	Southwest
SSE	South-southeast
WNW	West-northwest
NNW	North-northwest
Lat	Latitude
Lon	Longitude
s	Second
Hz	Hertz
m, km	Meter, kilometer
Vsmin250	Model with minimum Vs = 250 m/s
Vsmin500	Model with minimum Vs = 500 m/s

Supplementary Information

The online version contains supplementary material available at <https://doi.org/10.1186/s40623-023-01804-9>.

Additional file 1. The animation of total horizontal ground motion of the scattered wave field of the Osaka basin's response to the S-wave of the 1993/10/12 M_{JMA}7.1 event for Vsmin250 model and frequency range of 0.05–0.4 Hz. The lines originating at each of the stations show slowness vector of prevailing apparent wave propagation direction in the horizontal plane. The time is same as in Figures 4–7, the amplitude is normalized.

Additional file 2. The animation of total horizontal ground motion illustrating the complexity of the scattered wave field of the Osaka basin's response to the S-wave of the 1993/10/12 M_{JMA}7.1 event for Vsmin250 model and frequency range of 0–1 Hz. The shown surface size is SN x WE = 85 km x 90 km (without damping area). The time is same as in Figures 4–7, the amplitude is normalized.

Acknowledgements

In terms of the computer resources, this work was supported by the Ministry of Education, Youth and Sports (MEYS) of the Czech Republic through the e-INFRA CZ (ID:90140) of IT4Innovations Centre, Technical University, Ostrava. The seismic ground motion data in this study are observed by the temporal strong motion observations maintained by the authors of Hatayama et al. (1995).

Author contributions

IO contributed to conceptualization, analysis of the data and synthetics, coding the data processing software, interpretation of the results, visualization, and drafting the manuscript including figures. HS was involved in creation of the velocity model, supporting the research by knowledge of the local conditions, data curation, and supervision; TI contributed to conceptualization, creation of the velocity model, supporting the research by knowledge of the local conditions, data curation, approving the station positions and data, formal analysis, and supervision; JB was involved in methodology, draft corrections, enhancing paper by the interpretation of results, and supervision. All the authors read and approved the final manuscript.

Funding

This work was financially supported by Czech Science Foundation (GACR), project no. GA20-15818S; and by the Ministry of Education, Culture, Sports, Science and Technology (MEXT) of Japan, under its The Second Earthquake and Volcano Hazards Observation and Research Program (Earthquake and Volcano Hazard Reduction Research).

Availability of data and materials

The data shall not be shared, and they are not publicly available.

Declarations

Ethics approval and consent to participate

Not applicable.

Consent for publication

Not applicable.

Competing interests

The authors declare that they have no competing interests.

Author details

¹Institute of Geophysics of the Czech Academy of Sciences, Prague, Czech Republic. ²The Institute of Technology and Business in České Budějovice, České Budějovice, Czech Republic. ³Disaster Prevention Research Institute, Kyoto University, Gokasho, Uji, Kyoto, Japan.

Received: 26 September 2022 Accepted: 9 March 2023

Published online: 11 April 2023

References

- Asano K, Sekiguchi H, Iwata T, Yoshimi M, Hayashida T, Saomoto H, Horikawa H (2016) Modelling of wave propagation and attenuation in the Osaka sedimentary basin, western Japan, during the 2013 Awaji Island earthquake. *Geophys J Int* 204(3):1678–1694. <https://doi.org/10.1098/gji/ggv543>
- Beck JL, Hall JF (1986) Factors contributing to the catastrophe in Mexico City during the earthquake of September 19, 1985. *Geophys Res Lett* 13:593–596
- Bormann P (ed) (2012) New Manual of Seismological Observatory Practice (NMSOP-2). Potsdam, Deutsches GeoForschungszentrum GFZ; IASPEI. <https://doi.org/10.2312/GFZ.NMSOP-2>
- Burjánek J, Gassner-Stamm G, Poggi V, Moore JR, Fäh D (2010) Ambient vibration analysis of an unstable mountain slope. *Geophys J Int* 180(2):820–828. <https://doi.org/10.1111/j.1365-246X.2009.04451.x>
- Chaljub E, Moczo P, Tsuno S, Bard P-Y, Kristek J, Käser M, Stupazzini M, Kristekova M (2010) Quantitative comparison of four numerical predictions of 3D ground motion in the Grenoble valley. *France Bull Seismol Soc Am* 100(4):1427–1455. <https://doi.org/10.1785/0120090052>
- Dziewonski AM, Anderson DL (1981) Preliminary reference Earth model. *Phys Earth Planet Inter* 25:297–356
- Frankel A (1993) Three-dimensional simulations of ground motions in the San Bernardino valley, California, for hypothetical earthquakes on the San Andreas fault. *Bull Seismol Soc Am* 83(4):1020–1041. <https://doi.org/10.1785/BSSA0830041020>
- Fujino Y, Siringoringo D (2013) Vibration mechanisms and controls of long-span bridges: a review. *Struct Eng Inter* 23(3):248–268. <https://doi.org/10.2749/101686613X13439149156886>
- Furumura T, Hayakawa T, Nakamura M, Koketsu K, Baba T (2008) Development of long-period ground motions from the Nankai Trough, Japan, earthquakes: Observations and computer simulation of the 1944 Tonankai (Mw8.1) and the 2004 SE Off-Kii Peninsula (Mw7) Earthquakes. *Pure Appl Geophys* 165:585–607. <https://doi.org/10.1007/s00024-008-0318-8>
- Hatayama K, Matsunami K, Iwata T, Irikura K (1995) Basin-induced Love waves in the eastern part of the Osaka basin. *J Phys Earth* 43(2):131–155. <https://doi.org/10.4294/jpe1952.43.131>
- Hatayama K (2008) Lessons from the 2003 Tokachi-oki, Japan, earthquake for prediction of long-period strong ground motions and sloshing damage

- to oil storage tanks. *J Seismol* 12:255–263. <https://doi.org/10.1007/s10950-007-9066-y>
- Horikawa H, Mizuno K, Ishiyama T, Satake K, Sekiguchi H, Kase Y, Sugiyama Y, Yokota H, Suehiro M, Yokokura T, Iwabuchi Y, Kitada N, Pitarka A (2003) A three-dimensional subsurface structure model beneath the Osaka sedimentary basin, southwest Japan, with fault-related structural discontinuities. *Ann Report Active Fault Paleoequake Res Geol Survey Japan* 3:225–259 **(in Japanese with English abstract)**
- Irikura K, Kudo K, Okada H, Sasatani T (eds) (1998) The Effects of Surface Geology on Seismic Motion. *Proceedings of ESG'98*, December 1–3, 1998, Yokohama, Japan. Balkema, Rotterdam, ISBN 90 5809 030 2 (vol. 1–3), 1600 pp.
- Iwaki A, Iwata T (2008) Validation of 3-D basin structure models for long-period ground motion simulation in the Osaka basin, western Japan. *J Seismol* 12:197–215. <https://doi.org/10.1007/s10950-008-9088-0>
- Iwaki A, Iwata T (2010) Simulation of long-period ground motion in the Osaka sedimentary basin: performance estimation and the basin structure effects. *Geophys J Int* 181(2):1062–1076. <https://doi.org/10.1111/j.1365-246X.2010.04556.x>
- Iwaki A, Iwata T (2011) Estimation of three-dimensional boundary shape of the Osaka sedimentary basin by waveform inversion. *Geophys J Int* 186(3):1255–1278. <https://doi.org/10.1111/j.1365-246X.2011.05102.x>
- Iwata T, Asano K (2005) Long-period ground motion during the 2004 earthquake sequence off the Kii Peninsula and the Tokai District. *Zisin* 58(3):273–279. https://doi.org/10.4294/zisin1948.58.3_273
- Iwata T, Kagawa T, Petukhin A, Ohnishi Y (2008) Basin and crustal velocity structure models for the simulation of strong ground motions in the Kinki area, Japan. *J Seismol* 12:223–234
- Ismail M (2018) Seismic isolation of structures. Part I: Concept, review and a recent development. *Hormigón Acero* 69(285):147–161
- Kagawa T, Boming Z, Miyakoshi K, Irikura K (2004) Modeling of 3D basin structures for seismic wave simulations based on available information on the target area: case study of the Osaka Basin, Japan. *Bull Seismol Soc Am* 94:1353–1368. <https://doi.org/10.1785/012003165>
- Kawase H, Aki K (1989) A study on the response of a soft basin for incident S, P, and Rayleigh waves with special reference to the long duration observed in Mexico City. *Bull Seismol Soc Am* 79:1361–1382. <https://doi.org/10.1785/BSSA0790051361>
- Koketsu K, Hatayama K, Furumura T, Ikegami Y, Akiyama S (2005) Damaging long-period ground motions from the 2003 Mw 8.3 Tokachi-oki, Japan Earthquake. *Seismol Res Lett* 76(1):67–73. <https://doi.org/10.1785/gssrl.76.1.67>
- Koketsu K, Kikuchi M (2000) Propagation of seismic ground motion in the Kanto basin, Japan. *Science* 288:1237–1239
- Nakata T, Imaizumi T (2002) Digital active fault map of Japan. University of Tokyo Press, Tokyo (in Japanese), 60pp + 2 x DVD, <https://gbank.gsj.jp/ld/resource/geolis/200203687>. Accessed 24 Mar 2023
- Miyake H, Koketsu K (2005) Long-period ground motions from a large offshore earthquake: the case of the 2004 off the Kii peninsula earthquake. *Japan Earth Planets Space* 57(3):203–207
- Neidell NS, Taner MT (1971) Semblance and other coherency measures for multichannel data. *Geophysics* 36(3):482–497. <https://doi.org/10.1190/1.1440186>
- Oprsal I, Matyska C, Irikura K (2009) The source-box wave propagation hybrid methods: general formulation and implementation. *Geophys J Int* 176:555–564. <https://doi.org/10.1111/j.1365-246X.2008.03986.x>
- Oprsal I, Brokesova J, Faeh D, Giardini D (2002) 3D Hybrid Ray-FD and DWN-FD seismic modeling for simple models containing complex local structures. *Stud Geophys Geod* 46:711–730. <https://doi.org/10.1023/A:1021181422709>
- Oprsal I, Zahradnik J (2002) Three-dimensional finite difference method and hybrid modeling of earthquake ground motion. *J Geophys Res* 107(B8):16. <https://doi.org/10.1029/2000JB000082>
- Petersson NA, Sjögreen B (2012) Stable and efficient modeling of anelastic attenuation in seismic wave propagation. *Comm Comput Physics* 12(01):193–225
- Petersson NA, Sjögreen B (2015) Wave propagation in anisotropic elastic materials and curvilinear coordinates using a summation-by-parts finite difference method. *J Comput Phys* 299:820–841. <https://doi.org/10.1016/j.jcp.2015.07.023>
- Petersson NA, Sjögreen B (2017a) "User's guide to SW4, version 20". Technical report LLNL-SM-741439. Lawrence Livermore National Laboratory, Livermore, California, U.S.A.
- Petersson NA, Sjögreen B (2017b) SW4, version 2.01. *Comput Infrastr Geodyn*. <https://doi.org/10.5281/zenodo.1063644>
- Sekiguchi H, Masayuki Y, Horikawa H, Kunikazu Y, Kunimatsu S, Satake K (2008) Prediction of ground motion in the Osaka sedimentary basin associated with the hypothetical Nankai earthquake. *J Seismol* 12:185–195. <https://doi.org/10.1007/s10950-007-9077-8>
- Sekiguchi H, Yoshimi M, Asano K, Horikawa H, Saomoto H, Hayashida T, Iwata T (2013) Newly developed 3D velocity structure model of the Osaka sedimentary basin. *Abstracts of Japan Geoscience Union meeting*, Chiba, 19–24 May, 2013.
- Sekiguchi H, Asano K, Iwata T, Yoshimi M, Horikawa H, Saomoto H, Hayashida T (2016) Construction of a 3D Velocity Structure Model of Osaka Sedimentary Basin. *Proc. 5th IASPEI/IAEE Int. Symp. on the Effect of Surface Geology on Seismic Motion*, Taipei, August 15–17, 2016, paper P103B.

Publisher's Note

Springer Nature remains neutral with regard to jurisdictional claims in published maps and institutional affiliations.

Submit your manuscript to a SpringerOpen[®] journal and benefit from:

- Convenient online submission
- Rigorous peer review
- Open access: articles freely available online
- High visibility within the field
- Retaining the copyright to your article

Submit your next manuscript at ► [springeropen.com](https://www.springeropen.com)